Available online at www.sciencedirect.com
SCIENCE DIRECT®
ELSEVIER
International Journal of Solids and Structures 42 (2005) 5872–5886
INTERNATIONAL JOURNAL OF SOLIDS and STRUCTURES
www.elsevier.com/locate/ijsolstr

Design and modeling of an endoscopic piezoelectric tactile sensor

R. Sedaghati *, J. Dargahi, H. Singh

Department of Mechanical and Industrial Engineering, Concordia University, 1455 de Maisonneuve Blvd. West, Montréal, Québec, Canada H3G 1M8

Received 28 October 2004
Available online 13 April 2005

Abstract

The paper presents a proof-of-concept design of a tactile sensor capable of measuring compliance of a contact tissue/sensed object. The main objective of this study is to design and model a piezoelectric sensor capable of measuring the total applied force on the sensed object as well as its compliance. The sensor consists of a rigid and compliant cylindrical element. Determination of the compliance of sensed objects is based on the ratio of force experienced by the rigid cylinder to the total force applied to the sensor. To obtain this force ratio, a circular PVDF film is sandwiched between rigid cylinder and plate to measure the force applied on the rigid element and a rectangular PVDF film is sandwiched between the two base plates to measure the total force applied on the sensor. The detailed design of the senor was performed using finite element analysis. A prototype was fabricated and tested and it has been shown that good agreement exists between the finite element results and experimental values. The proposed sensor exhibits high force sensitivity and good linearity and offers the potential for future miniaturization in order to be integrated with the commercial endoscope graspers used in minimally invasive surgery.

Keywords: Piezoelectric; Tactile sensor; Design; Finite element analysis; Endoscopic grasper

1. Introduction

In present days, application of engineering concepts to the instruments designing for the medical purposes are challenging and demanding. The main objective of this research work is to design the prototype

* Corresponding author. Tel.: +1 514 848 7971; fax: +1 514 848 8635.
E-mail address: sedagha@alcor.concordia.ca (R. Sedaghati).

0020-7683/$ - see front matter © 2005 Elsevier Ltd. All rights reserved.
doi:10.1016/j.ijsolstr.2005.03.029

piezoelectric sensor for the force and compliance measurement of the tissue. The senor can be miniaturized to integrate with the commercial endoscope graspers used in minimally invasive surgery (MIS).

MIS is a revolutionary surgical technique in which the surgery is performed with the fine instruments and viewing equipment inserted through small incisions rather than by making a large incision to expose and provide access to the operation site. The main advantage of this technique is reduced trauma to the healthy tissue, which is a leading cause for patient postoperative pain and long hospital stay. The less hospital stay and rest periods also reduce the cost of surgery. However MIS procedures are more demanding on the surgeon, requiring more difficult surgical techniques.

Minimally invasive surgery operations include laparoscopy, thoracoscopy, arthroscopy, ophthalmic micro-surgery etc. Muhe, German scientist, performed the first major laparoscopic surgery for gall bladder removal in 1985. In less than 10 years, there was a quick shift from open surgery to laparoscopic surgery in the United States of America (Tendick et al., 1995). Adoption of laparoscopic techniques is slower in more complex procedures, largely because of the greater difficulty due to the surgeon's reduced dexterity and perception.

One of the main problems in a typical MIS is a lack of tactile sensation on which surgeon can highly depend during the surgery to locate arteries and tumors hidden in the tissue. Also, softness of the tissue cannot be judged during the operation using ordinary instruments. In other words, to perform the MIS more effectively, the surgeon should be able to feel the tissue, sensing the pressure of blood vessels and ducts during the procedure. This ability is very important during manipulation tasks such as the grasping of the internal organs, gentle load transfer during lifting, suturing and removing tissues. The need to feel the tissue and its softness is particularly important during operation. In MIS surgery, stereoscope vision and tactile information about tissue consistency are no longer available to the surgeon. To compensate for these sensory deficits, various tissues can be characterized with an electromechanical sensor that records their properties. Then the array of these sensors can be integrated with the surgical instruments, providing the surgeon with information about tactile properties of tissue.

In laparoscopy, long slender tools are inserted through small puncture openings in the abdominal wall and the surgeon uses a range of tip-mounted instruments guided by video feedback images. Since, the instruments are rigid rods and effectively have fixed pivots at the entry points, the available degrees of freedom are restricted and therefore demand extra operator expertise. Voges (1996) reports the main difficulties experienced during the endoscopic surgery: restricted manipulation mobility, lack of depth from 2D vision and the almost complete lack of a sense of touch. Voges provides the relevance of tele-presence and predicts the future setup with a new design of flexible instruments having greater mobility, force reflection, 3D monitoring and data enhancement. Commercial available endoscopic grasper do not have any tactile sensor, hence, the surgeon do not have any tactile feedback. One of the most important aspects in MIS is the palpation evaluation to determine the compliance/softness of a contact tissue. Many researchers performed the work on tactile feedback and force measuring device for the endoscopic grasper. Dario (1991) short but farsighted review cites medical applications in which the hardness of soft tissues is detected through palpation. Mehta et al. (1996) has designed and fabricated a micro-machined tooth-like endoscopic pressure sensor. However, the sensor could only measure a few grams of a force. Gray and Fearing (1996) report on an array of micro-machined capacitive tactile sensor. However it has been shown some hysteresis problem. Some sensors have been proposed to measure the compliance of the tissue. Bicchi et al. (1996) have measured compliance and viscoelastic property of tissues by measuring the force and angular displacement of endoscopic graspers. A micro-robot designed for colonoscopy and using a pneumatic inchworm propulsion method is described by Dario et al. (1997). Dario et al. (1988) have constructed a tactile sensor, which can differentiate various complaint objects. But their work lacks any theoretical basis. An experiment with a sensor for laparoscopic attachment has been described by Fischer et al. (1995). A 64-point sensor of area 1 cm^2 was connected to a fingertip for vibrotaction display.

Cohn et al. (1995) discussed about the series of designs for endoscopic and laparoscopic tools, that intended incorporating their tactile tele-presence apparatus. An interesting idea raised here is the possibility of using the capacitive tactile sensor, not to measure applied force, but to detect the varying dielectric permittivity of different tissue. It was reported that water, fat, blood vessels, and cancerous tissue might all be differentiated by this means. A striking feature of the design of Umemori et al. (1996) is that it uses disposable kit with the help of inexpensive materials, and in this case sensing head is replaced for each patient. This aspect is very important for medical sensors to avoid infection and transmitted diseases.

In the following sections, a short description of the sensor design is presented. This is followed by a description of the finite element models and experimental studies. The finite element and experimental results are discussed and compared. At the end conclusion and scope for future improvement are provided.

2. Sensor design

A single sensor capable of measuring the applied force on the tissue and softness of the tissue has been designed and fabricated. It mainly consists of two cylinders. One cylinder (compliant cylinder) is significantly more flexible than the other cylinder (rigid cylinder). The rigid cylinder is glued to the base plate and surrounded with the compliant cylinder. The rigid and compliant cylinders are made up of phenolic and soft rubber, respectively. The PVDF films are used for measuring the forces at the rigid and complaint part of the sensor. One circular PVDF film is placed between the rigid and base plate, and the other PVDF film is sandwiched between the two rigid plexiglas plates. The PVDF film placed between the two plates measures the total force applied on the tissue, PVDF between rigid and base plate measures the force experienced by the rigid part. An array of these sensors could be designed in a miniaturized form and it can be integrated with commercial endoscopic grasper.

The sensor consists of a rigid cylinder surrounding by a compliant cylinder. The rigid and compliant cylinder is made up of the phenolic and soft rubber, respectively. A 25 μm circular PVDF film with radius of 1.4 mm is sandwiched between the rigid cylinder and base plate which measures the force applied to the rigid cylinder. Also a 25 μm × 10 mm × 10 mm rectangular PVDF film is placed between the two base plexiglas plates to measure the total applied load. Coaxial wires are used to carry signal to a charger amplifier through channel groove in upper and lower base plexiglas plates. The conductive and non-conductive epoxy glue and urethane glue have been used for the required attachments. The design and the relative dimensions of the single sensor are shown in Fig. 1a. Fig. 1b shows the fabricated prototype of the single sensor. The white circular shape in the photograph shows the rigid cylinder while the black colored outer part is the compliant cylinder. The mechanical properties of the different parts of the proposed single sensor are provided in Table 1.

3. Finite element formulation

The finite element method is used to study the force reaction on the complaint and rigid parts of sensor. Tissue is also modeled in the analysis, and the assumption was made that tissue has uniform distributed modulus of elasticity and show linear behavior. Two distinct finite element approaches have been used to simulate the behavior of the sensor under uniform applied load. First an efficient 2D finite element model based on the elasticity approach has been proposed to study the response characteristics of the sensor and then 3D finite element model of the sensor has been developed in ANSYS and the results are compared with the proposed 2D model.

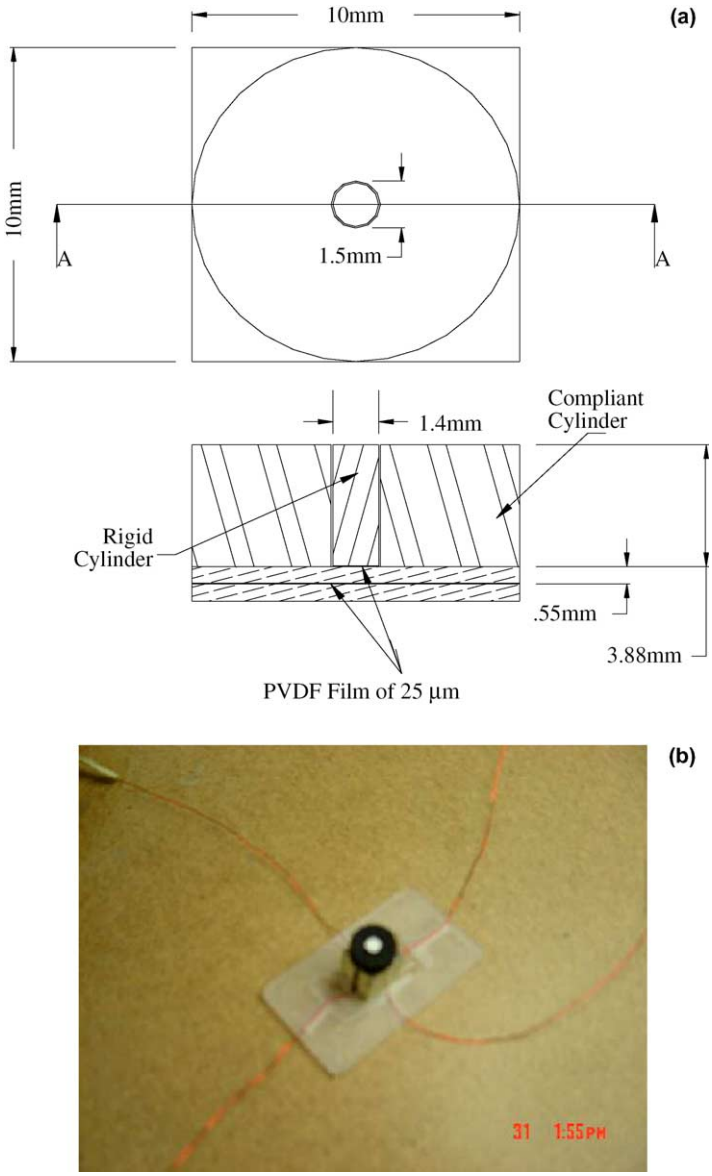

Fig. 1. (a) The design of the single sensor. (b) The fabricated single sensor.

3.1. 2D finite element model

In this model, the rigid cylindrical part is considered as rigid support and there is no deflection in the rigid cylindrical part. Only the compliant cylinder part and tissue are considered flexible and can deflect under very small external load. For the finite element model, the tissue has been modeled as a beam on rigid (rigid cylinder) and elastic foundation (compliant cylinder). The compliance of the sensed object (tissue) has been calculated by measuring the force distribution on the rigid and compliant parts. The higher the tissue

Table 1
Properties of the materials used in the single sensor

Name of part	Young's modulus
Plexiglas base plates	70×10^6 Pa
Compliant cylinder	2.4×10^4 Pa
Rigid cylinder	10 GPa
Circular PVDF film	1.8–2.7 GPa
Rectangular PVDF film	1.8–2.7 GPa

modulus the more reaction will be on the rigid cylinder. It is noted that the relative deflection between the rigid and compliance part enables the sensor to act as a tooth for holding the tissue.

Due to the symmetry, only half of the sensor has been investigated. The proposed finite element model has been shown in Fig. 2 in which the sensed object has been discretised into two beam elements.

A uniform load is applied to the sensed object (tissue). The potential energy for the beam on an elastic foundation can be written as (Bathe, 1996):

$$\pi = \int_0^L \frac{EI}{2}\left(\frac{\mathrm{d}^2 v}{\mathrm{d}x^2}\right)^2 \mathrm{d}x + \int_0^L \frac{k_f v^2}{2}\mathrm{d}x - \int_0^L Pv\,\mathrm{d}x \tag{1}$$

where $v(x)$ is the displacement function, E and I are young's modulus and second moment of inertia respectively, k_f is the spring constant per unit length and P is the uniform load applied on the beam. The displacement function, $v(x)$, can be related to the element nodal displacement vector as

$$v(x) = \{N\}^{\mathrm{T}}\{u\} \tag{2}$$

where $\{N\}$ and $\{u\}$ are the shape function and nodal displacement vectors, respectively. The shape function vector for the flexural beam element can be written as $\{N\}^{\mathrm{T}} = [N_1\, N_2, N_3\, N_4]$ where shape functions N_1, N_2, N_3 and N_4 can be described as:

$$N_1 = \frac{2x^3 - 3x^2L + L^3}{L^3}, \quad N_2 = \frac{x^3L - 2x^2L^2 + xL^3}{L^3}, \quad N_3 = \frac{-2x^3 + 3x^2L}{L^3}, \quad N_4 = \frac{x^3L - x^2L^2}{L^3} \tag{3}$$

By substituting Eq. (2) into Eq. (1) and we may obtain:

$$\Pi = \frac{1}{2}EI\int_0^L \{u\}^{\mathrm{T}}[B]^{\mathrm{T}}[B]\,\mathrm{d}x\{u\} + \frac{1}{2}\int_0^L k_f\{u\}^{\mathrm{T}}[N]^{\mathrm{T}}[N]\,\mathrm{d}x\{u\} - \int_0^L P\{u\}^{\mathrm{T}}[N]^{\mathrm{T}}\,\mathrm{d}x \tag{4}$$

where $[B] = \frac{\partial^2[N]}{\partial x^2}$, represented as

$$[B] = \left[\frac{12x - 6L}{L^3} \quad \frac{6xL - 4L^2}{L^3} \quad \frac{-12x + 6L}{L^3} \quad \frac{6xL - 2L^2}{L^3}\right] \tag{5}$$

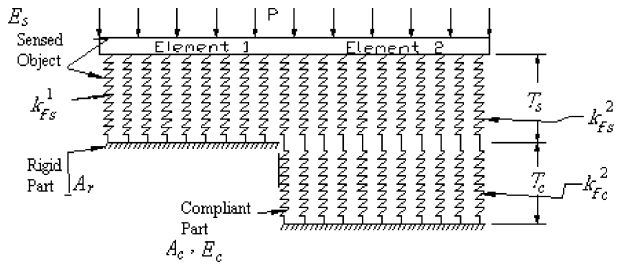

Fig. 2. Proposed finite element model for the single tactile sensor.

Differentiating Eq. (4) with respect to {u}, the equilibrium equation can be written as:

$$\frac{\partial \Pi}{\partial\{u\}} = EI\int_0^L [B]^{\mathrm{T}}[B]\,\mathrm{d}x\{u\} + \int_0^L K_f[N]^{\mathrm{T}}[N]\,\mathrm{d}x\{u\} - \int_0^L P[N]^{\mathrm{T}}\,\mathrm{d}x = 0 \tag{6}$$

or

$$\left[EI\int_0^L [B]^{\mathrm{T}}[B]\,\mathrm{d}x + \int_0^L k_f[N]^{\mathrm{T}}[N]\,\mathrm{d}x\right]\{u\} = \int_0^l P[N]^{\mathrm{T}}\,\mathrm{d}x \tag{7}$$

Eq. (7) can be written in matrix form as:

$$[k]\{u\} = \{f\} \tag{8}$$

where $[k]$ is the element stiffness matrix and $\{f\}$ is the element nodal force vector and can be expressed as:

$$[k] = EI\int_0^L [B]^{\mathrm{T}}[B]\,\mathrm{d}x + \int_0^L k_f[N]^{\mathrm{T}}[N]\,\mathrm{d}x \tag{9}$$

$$\{f\} = \int_0^L P[N]^{\mathrm{T}}\,\mathrm{d}x \tag{10}$$

It is noted that the stiffness matrix has two terms. The first term is the regular stiffness matrix of the beam and the second term is the stiffness matrix due to the elastic foundation. In other words:

$$[k] = [k_{\text{beam}}] + [k_{\text{elastic foundation}}] \tag{11}$$

where

$$[k_{\text{beam}}] = EI\int_0^L [B]^{\mathrm{T}}[B]\,\mathrm{d}x \tag{12}$$

$$[k_{\text{elastic foundation}}] = \int_0^L k_f[N]^{\mathrm{T}}[N]\,\mathrm{d}x \tag{13}$$

Substituting the matrices $[B]$ and $[N]$ from Eqs. (3) and (5) into Eqs. (12) and (13), we can obtain:

$$[k_{\text{beam}}] = \frac{EI}{L^3}\begin{bmatrix} 12 & 6L & -12 & 6L \\ 6L & 4L^2 & -6L^2 & 2L^2 \\ -12 & -6L^2 & 12 & -6L \\ 6L & 2L^2 & -6L & 4L^2 \end{bmatrix} \tag{14}$$

$$[k_{\text{elastic foundation}}] = k_f\begin{bmatrix} \frac{13L}{35} & \frac{11L}{210} & \frac{9}{70} & \frac{-13L}{420} \\ \frac{11L}{210} & \frac{L^2}{105} & \frac{13L}{420} & -\frac{L^2}{140} \\ \frac{9}{70} & \frac{13L}{420} & \frac{13}{35} & -\frac{11L}{210} \\ \frac{-13L}{420} & -\frac{L^2}{140} & -\frac{11L}{210} & \frac{L^2}{105} \end{bmatrix} \tag{15}$$

$$\{f\} = \frac{PL}{12}\begin{Bmatrix} -6 \\ L \\ -6 \\ -L \end{Bmatrix} \tag{16}$$

After assembling the two elements, the equilibrium equation at the system level can be written as:

$$[K]\{U\} = \{F\} \tag{17}$$

where $[K]$, $\{U\}$ and $\{F\}$ are the system stiffness matrix, system nodal displacement and system nodal force vectors, respectively.

The equivalent spring constant k_f for element number 2 in Fig. 4 is obtained by the fact that the sensed object and the compliant material are connected in series (two springs in series). Thus the equivalent spring constant k_f for element 1 and 2, k_f^1 and k_f^2, can be described as:

$$k_f^1 = k_{fs}^1 \tag{18}$$

$$k_f^2 = \frac{k_{fs}^2 k_{fc}}{k_{fs}^2 + k_{fc}} \tag{19}$$

where k_{fs}^1 and k_{fs}^2 are the spring constants per unit length of the sensed object related to the elements 1 and 2, respectively and k_{fc} is the spring constant per unit length of the compliant cylinder and can be explained as follows:

$$k_{fs}^1 = \frac{A_r \times E_s}{T_s}, \quad k_{fs}^2 = \frac{A_c \times E_s}{T_s}, \quad k_{fc} = \frac{A_c \times E_c}{T_c} \tag{20}$$

where A_r, A_c, T_c, E_c, T_s and E_s are the cross-sectional area of the rigid cylinder, cross-sectional area, thickness and Young's modulus of the compliant cylinder and thickness and Young's modulus of the sensed object, respectively. It is again noted that during the calculation of the stiffness matrix related to the elastic foundation in Eq. (15), the spring constant per unit length k_f would be equal to k_f^1 for element 1 and equal to k_f^2 for element 2.

Substituting Eq. (20) into Eqs. (18) and (19), we may obtain:

$$k_f^1 = \frac{A_r \times E_c}{T_c}\lambda \tag{21}$$

$$k_f^2 = \frac{A_r E_c}{T_c}\frac{\lambda A}{(1+\lambda)} \tag{22}$$

where λ and A are dimensionless parameters which are defined as:

$$\lambda = \frac{E_s T_c}{E_c T_c}, \quad A = \frac{A_c}{A_r} \tag{23}$$

Considering Eqs. (21) and (22), it can be realized that the force ratio (the force experienced by the rigid cylinder to the total force applied to the sensor) is a function of dimensionless parameters, λ and the area ratio A. Using above formulation, a finite element analysis has been performed to find the force ratio variation with respect to dimensionless parameter λ. The results obtained for the different area ratio, A, are shown in Fig. 3.

As the parameter λ increases, the sensed object becomes stiffer than the compliant cylinder of the sensor. It is interesting to note that in the limit where the sensed object is very stiffer than the compliant cylinder, the force ratio will be unity. When stiffness of the sensed object nearly equals to the rigid cylinder, only the

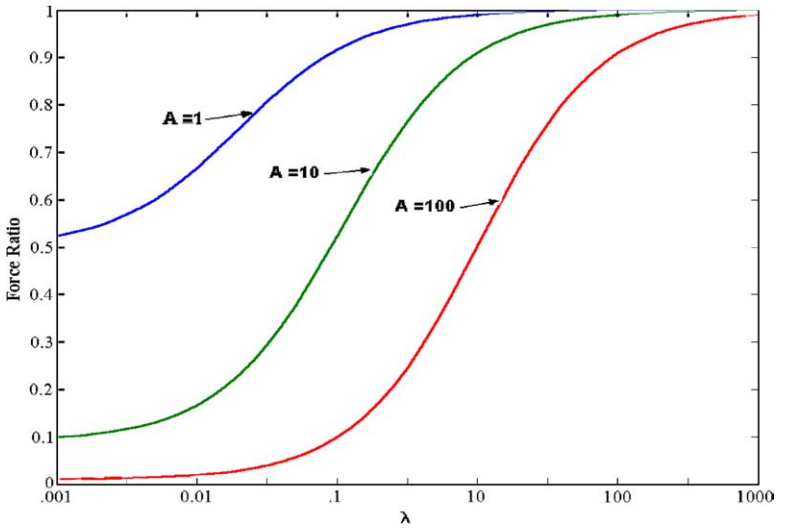

Fig. 3. Variation of the force ratio with the lambda function at different area ratios.

rigid cylinder carries all the forces applied. On the other hand, when the sensed object is softer as compared to the compliant cylinder, the outer compliant cylinder carries most of the force. As a result of this the force ratio decreases. As it can be seen from Fig. 3, force ratio also depends on the area ratio. The larger the area ratio, the larger the variation in the force ratio, thus the compliance of the sensed object can be better estimated in a wide range. It is noted that in this simulation the Young's modulus of the compliant cylinder and the thickness of the both sensed object and the compliant cylinder, which their effect can be realized in parameter λ, are assumed to be fixed. However in general the force ratio also depends on these parameters.

3.2. 3D finite element model using ANSYS

The sensor has also been modeled in ANSYS to validate the results obtained from the proposed finite element model. Due to the electromechanical nature of the problem, different types of elements have been employed to construct the finite element model of the senor. These elements and the three-dimensional model of the sensor are shown in Figs. 4 and 5, respectively. Element Solid 45 has been used to model the plate 1, plate 2 and sensed object of the sensor. The irregular and curved parts of sensor, the rigid and compliant cylindrical parts are all modeled using element Solid 92. Element Solid 5 has been used to mesh the straight edge geometries and rectangular PVDF film which measures the total force of sensor. Element Solid 98, which has a piezoelectric and structural field capabilities similar to Solid 5, is well suited to model irregular edges and has been employed to model the circular PVDF films.

It is noted that the force response of the sensor using 3D finite element model has also been obtained for uniform pressure load applied on the sensed object in order to be able to compare the results with those of 2D model. Results obtained from the 3D ANSYS formulation are compared with those of 2D model. The comparison between the proposed 2D formulation and 3D ANSYS model has been shown in Fig. 6. It is noted that both 2D and 3D models follow the similar pattern. The area ratio of the sensor is 11.60. It should be emphasized that the lambda parameter is a function of the thickness and Young's modulus of both compliant cylinder and sensed object and thus the variation of any of these parameters will affect the lambda.

In this study it is assumed that the thickness of the compliant cylinder and its modulus of elasticity and also thickness of the sensed object are constant. Therefore the variation of the lambda can only be

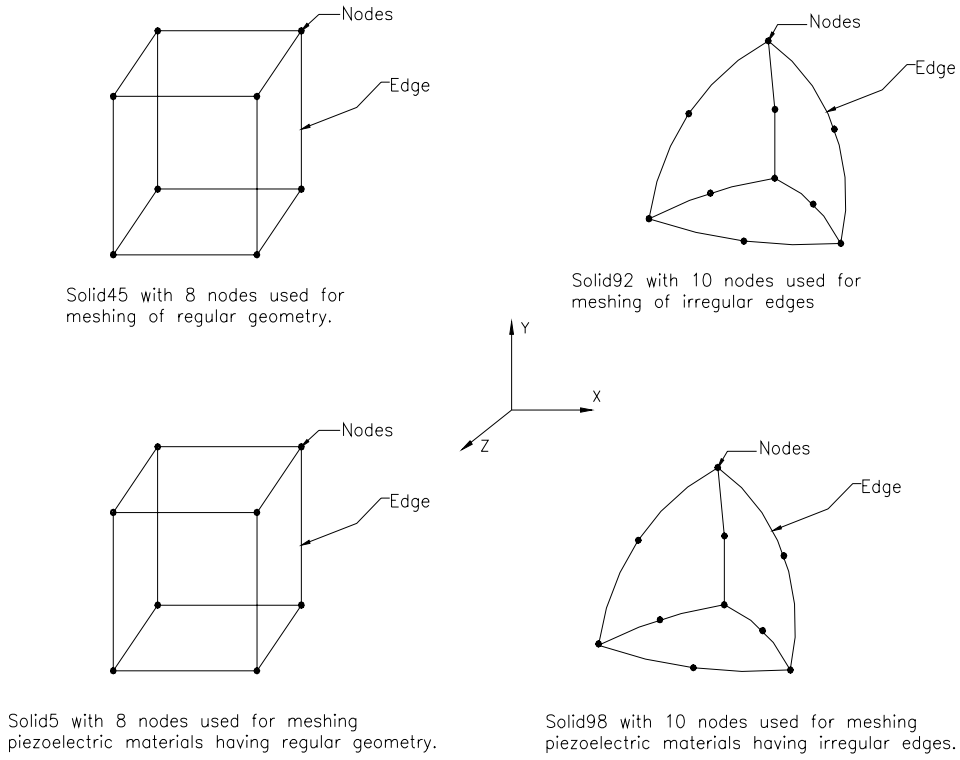

Fig. 4. Different types of elements used for meshing.

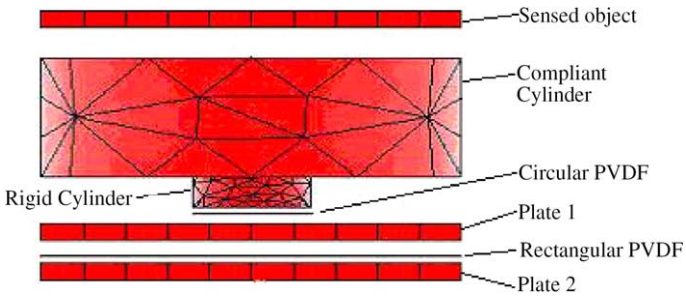

Fig. 5. Meshed single sensor with assigned elements.

attributed to the modulus of the sensed object. Considering this, variation of force ratio can be directly studied with respect to modulus of elasticity of the sensed object. Fig. 7 demonstrates this variation for 2D and 3D model of single sensor for two different compliant cylinder materials.

4. Experimental setup

The layout of the experimental setup and its photograph are shown in Fig. 8a and b, respectively. A power amplifier has been used to condition signal generated by the signal generator. That conditioned

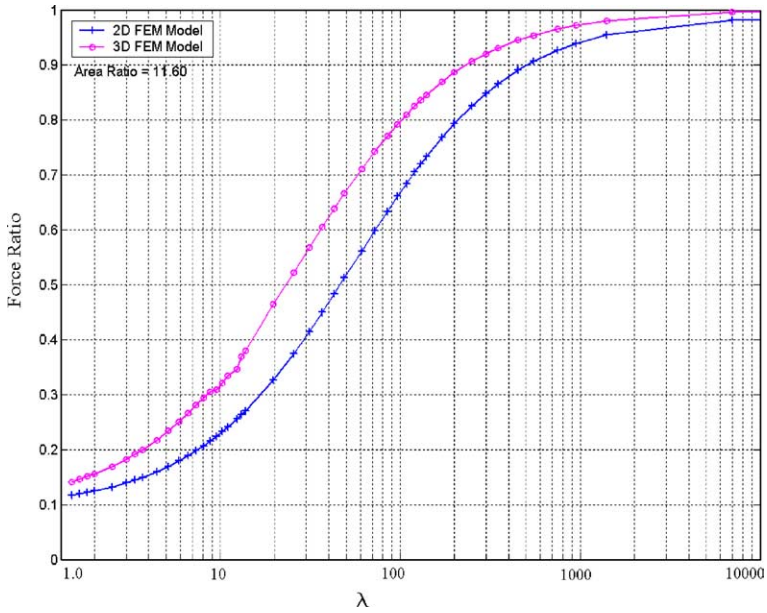

Fig. 6. Force ratio versus λ for the 2D and 3D FEM models.

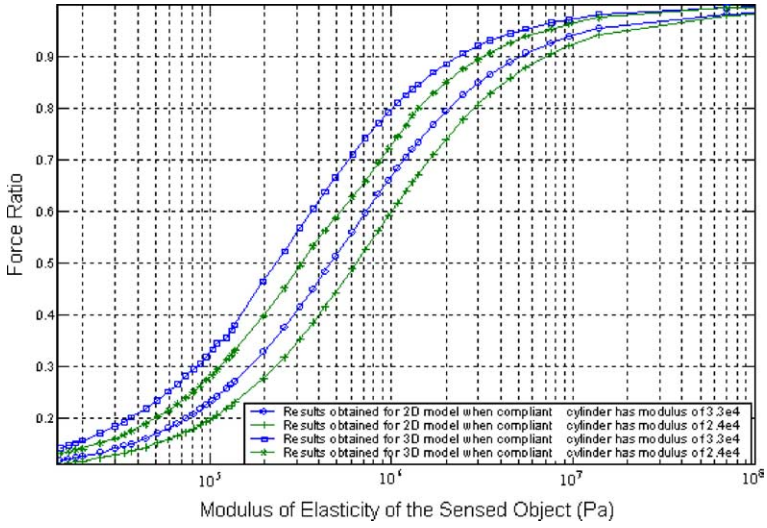

Fig. 7. Comparison of the 2D and 3D FEM models of single sensor results for different complaint cylinders.

signal is then used to drive vibrator. A sinusoidal signal with the frequency of 10 Hz has been used in these experiments. Tactile sensors should be capable of measuring the frequency of sensor from range 0 Hz to 20 Hz. This range depends upon the application of the tactile sensor. It is noted that in the actual practice, the working frequency of the tactile sensor is around 10 Hz. A micro-positioner has been used to position the sensor relative to the position of the probe. Both static load and dynamic applied load measured through the load cell, positioned between the probe and the shaker. The signal obtained from the tactile sensor is directed to the charger amplifier for the required amplification and measured on an oscilloscope.

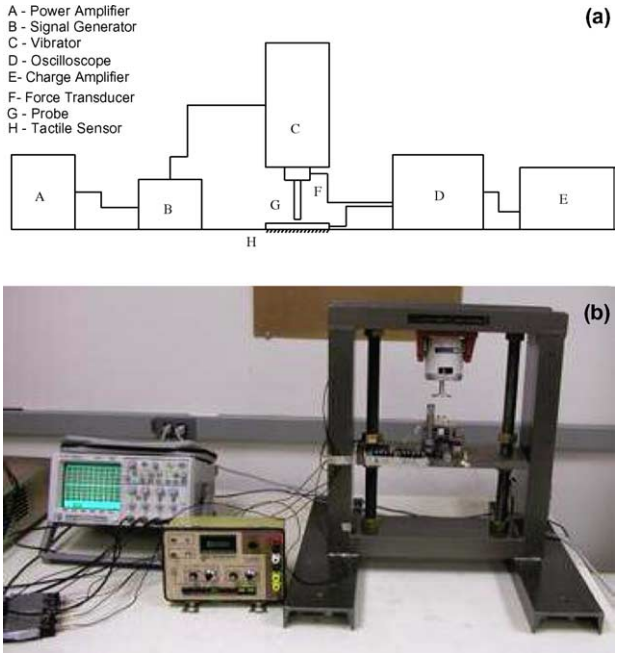

Fig. 8. (a) Layout of the experimental setup for measuring the response of the tactile sensor. (b) Experimental setup used to measure the response of the tactile sensor.

The signal of the vibrator and amplified signal of tactile sensor are monitored in an oscilloscope. It is noted that all the required instruments have been calibrated properly.

4.1. Measurement of modulus of elasticity of the sensed objects

The modulus of elasticity of the sensed object has been measured by applying load and measuring strain. This was done by using the load cell and a circular probe of radius 1 cm. Circular specimens were cut into the same size as the diameter of the probe. The readings from the micro-positioner and strain gage meter provided the deflection and load on the specimen, respectively. Six rubber samples were used. Out of these rubber samples, properties of the five samples are known (samples 1–5) and one unknown (sample 6). The rubber samples are numbered as 1–6. The specimens of 1 cm radius and 3 mm thickness have been used.

Before starting the experiment, it is extremely necessary to calibrate the instruments and find the sensitivity of the load cell. The calibration of the load cell was carried out using standard weights. First, the load cell was mounted on the vibrator, then the output is fed into the strain gage meter for measurement. The sensitivity of the strain indicator has been found to be about 0.1053 mV/g.

The experimental values of the modulus of elasticity under compression deflection test obtained from the experimental results have been compared with the known technical data provided by the manufacturer. It is found that good correlation exists between the experimental results and the known data within the range of compression test provided by the manufacturer. For instance the value of the experimental compression test for sample 1 are found to be between 109.8 kPa and 114.5 kPa, which exactly lies between the range of the 82.8–137.8 kPa provided by the manufacturer as shown in Table 2. The test has also been conducted on the unknown sample 6 and its modulus of elasticity was found to be around 102.59 kPa.

The expected order of the softness is shown in Fig. 9 based on the calculated values of the modulus of elasticity. These values are also in correlation within the range given by the manufacturer. Sample 1 is

Table 2
Modulus of elasticity (kPa) of the rubber specimens provided by the manufacturer

Sample no.	1	2	3	4	5
Polymer	Silicone	Neoprene	NBR/PVC/NEO blend	Natural	NBR/PVC/NEO blend
Compression test	82.8–137.8	13.8–34.5	27.6–55.2	20.7–34.5	20.7–34.5
Tensile test	344	517	517	173–186	344

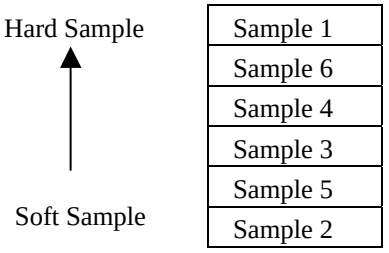

Fig. 9. Expected order of the softness of the samples.

supposed to be at the top and sample 2 is at the extreme bottom. Sample 6 is placed in the softness order based on the calculated softness values obtained experimentally.

4.2. Experimental results

The experimental tests have been conducted on the fabricated sensor. The sensor is mounted on the micro-positioner that is placed beneath the load cell. The rubber samples with area of 1 cm^2 have been used as the sensed objects and sandwiched between the probe and the sensor. Readings at the different load have been recorded in order to obtain the variation of the force ratio. Six load sets have been used and each sample has been tested under different load set to confirm the force ratio of the rigid part to the total force applied. In samples 1 and 6 (hard samples), sinusoidal output is very clear without any noise disturbances. On the other hand, samples 2 and 5 show some noise in the output. This is mainly due to this fact that the soft rubbers are compressed more under small load and acted as vibration damper for the sinusoidal input.

A typical data for the single PVDF sensor at 3 N load are provided in Table 3. The results confirm that different forces are experienced by the rigid part and compliant part and they vary proportionally. The output voltages from the PVDF films are measured in millivolts on the oscilloscope. From the force ratio, the compliance of the sample can be extracted. The higher the force ratio the more rigid is the sample and vice

Table 3
Experimental results for the single sensor

Experimental data at load 3 N							
Sample no.	Load (g)	Meter reading (mV)	Circular cylinder PVDF (mV)	Rectangular PVDF (mV)	Force rigid (N)	Total force (N)	Force ratio
1	305.8	32	5.87	213	0.964	3.074	0.329
2	305.8	32	2.484	206	0.432	3.121	0.139
3	305.8	32	3.290	212	0.573	3.212	0.178
4	305.8	32	4.304	218	0.742	3.334	0.223
5	305.8	32	2.983	200	0.514	3.059	0.168
6	305.8	32	5.018	214	0.873	3.088	0.283

versa. It is noted that appropriate calibration has been conducted on both rectangular and circular PVDF films in order to obtain the force experienced by the rigid part and the total force, respectively from the relative output voltages.

5. Comparison of the theoretical and experimental results

The results obtained from the experimental setup are compared with the theoretical results discussed before in Section 3. It is again noted that the thickness of the sensed object and compliant cylinders and the Young's modulus of the compliant cylinder are kept constant. Thus the parameter λ only depends on the modulus of the sensed object. The results obtained from 2D and 3D models of the single sensor are compared with the experimental results as shown in Fig. 10. It can be seen that the experimental results show good linearity and are in good agreement with the theoretical results. It is also interesting to note that the experimental results obtained from prototype single sensor are bounded by the results obtained from 2D and 3D finite element model. The deviation between experimental and theoretical results can be attributed to the non-linear elastic nature of the rubber, which has not been addressed in the finite element models. The average percentage error with respect to the 3D model is about -7%.

It is noted that the softness order of materials judged by the sensor is in agreement with the expected softness order of materials irrespective of the percentage errors.

6. Tooth-like sensor

The proposed sensor design can also act like tooth for holding the slippery tissues (sensed objects). This characteristic is not available in the conventional tactile endoscopic sensors. As discussed the measurement of the compliance of the sensed objects was based on the relative deformation of the compliance part. The relative deformation gives different force experienced by rigid and compliant part. The relative deformation of the parts varies with the force ratio. The higher is the force ratio less will be the relative deformation.

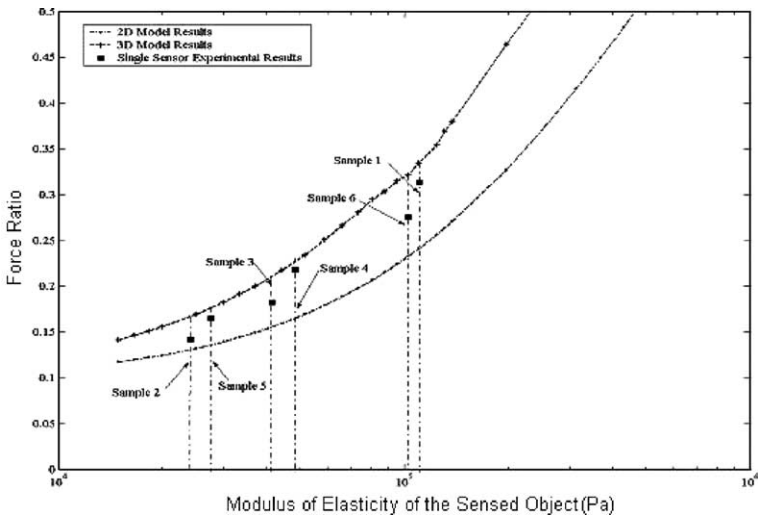

Fig. 10. Comparison of the theoretical and experimental results for the single sensor.

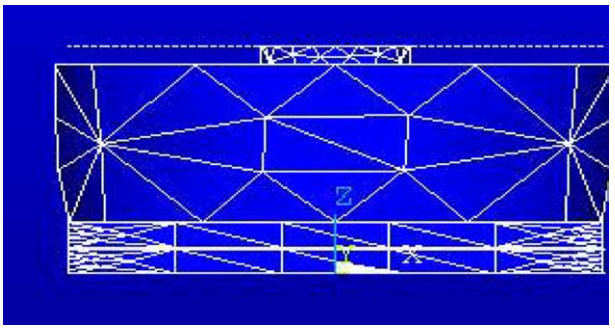

Fig. 11. Single sensor acting like tooth.

When the force is applied to the sensor, the compliant part deforms and the rigid part remains un-deformed. Due to this behavior, the rigid part protrudes outward and acts as teeth. The protruded rigid part of sensor is shown in Fig. 11. In this case there is no need to create artificial teeth on the sensor for grasping purposes. The number of teeth depends on the sensor count. The size of the endoscopic grasper varies from few centimeters depending upon the requirement and purpose of the grasper.

In the future it is aimed to miniaturize the proposed sensors on the endoscopic graspers. The rigid cylinder serves the purpose of the tooth during the holding of object. Increasing the number of rigid cylinders will provide good holding properties and also provide more reliable results.

7. Conclusion

The paper presents a proof-of-concept design of an endoscopic piezoelectric tactile sensor. The main objective of this study is to design and model a piezoelectric sensor capable of measuring the total applied force on the sensed object as well as the compliance of the tissue/sensed object.

A finite element model has been proposed to study the performance of tactile sensors. The sensed object has been modeled as an elastic beam on rigid and elastic foundations and the results are compared with 3D ANSYS model. The compliance of the sensed object is measured by recording the PVDF films response under different load sets. A single sensor have been designed and fabricated in order to validate the simulation results. It is shown that good agreement exist between theoretical and experiment results. All the results are obtained on the large-scale tactile sensors. The proposed sensors can be integrated on the endoscopic grasper, thus accurate measurement and high precision is very important. To integrate these sensors with endoscopic grasper, miniaturization is required which is not studied here. Miniaturization will reduce the deformation and shearing effect in the sensed object. The system either large or small could be damaged by large shear force on the sensor surface due to slipping of the sensed object from the endoscopic grasper. Further investigation is required to overcome this problem.

The tissue (sensed object) encountered in endoscopic has a high nonlinear characteristic, with a time dependent constitutive relation. Future study is required to account for this viscoelastic behavior.

References

Bathe, K.J., 1996. Finite Element Procedures. Prentice-Hall.

Bicchi, A., Canepa, G., De Rossi, D., Iaccconi, P., Scilingo, E.P., 1996. A sensorized minimally invasive surgery tool for detecting tissue elastic properties. In: Proceedings of the IEEE International Conference on Robotics and Automation, Minneapolis, Minnesota, April.

Cohn, M.B., Crawford, L.S., WendLandt, J.M., Sastry, S.S., 1995. Surgical application of milli robots. Robotics Systems 12 (6), 401–416.

Dario, P., 1991. Tactile sensor—technology and applications. Sensor and Actuators A—Physics 26, 251–256.

Dario, P., Bergamasco, M., Sebatini, A., 1988. Sensing body structure by an advanced robotic systems. In: Proceedings of the IEEE International Conference on Robotics, pp. 1758–1763.

Dario, P., Carrozza, M.C., Lencoini, L., Maganani, B., D'Attanasio, S., 1997. A micro robotics system for colonoscopy. In: Proceedings of the IEEE International Conference on Robotics and Automation, Albuquerque, New Mexico, April, pp. 1567–1572.

Fischer, H., Neisius, B., Trapp, R., 1995. Tactile feedback for endoscopic surgery. In: Morgan, K., Satava, R.M., Sieburg, H.B., Mattheus, R., Christensen, J.P. (Eds.), Interactive Technology and a New Paradigm for Health Care. IOS press, Newport Beach, CA.

Gray, B.L., Fearing, R.S., 1996. A surface micro-machined micro tactile sensor array. In: Proceedings of the IEEE International Conference on Robotics and Automation, Minneapolis, Minnesota, April.

Mehta, M., 1996. A Micromachined Capacitative Pressure Sensor for Use in Endoscopic Surgery. M.Sc. Thesis, School of Engineering Science, Simon Fraser University, BC, Canada.

Tendick, F., Mori, T., Way, L., 1995. The future of laparoscopic surgery. In: Way, L., Bhoyrul, S., Mori, T. (Eds.), Fundamentals of Laparoscopic Surgery. Churchill-Livington, Pittsburg, PA.

Umemori, M., Sugawara, J., Kawauchi, M., Mitani, H., 1996. A pressure-distribution sensor (PDS), for evaluation of lips functions. American Journal of Orthodontics and Dentofacial Orthopedics 109, 473–480.

Voges, U., 1996. Technology in paparoscopy—what to expect in the future. Urology Ausgabe (a) 35, 208–214.